
LEARNING A MESH MOTION TECHNIQUE WITH APPLICATION TO FLUID-STRUCTURE INTERACTION AND SHAPE OPTIMIZATION *

Johannes Haubner, Miroslav Kuchta

Department of Numerical Analysis and Scientific Computing
Simula Research Laboratory
Oslo, Norway
{haubnerj,miroslav}@simula.no

Abstract

Mesh degeneration is a bottleneck for fluid-structure interaction (FSI) simulations and for shape optimization via the method of mappings. In both cases, an appropriate mesh motion technique is required. The choice is typically based on heuristics, e.g., the solution operators of partial differential equations (PDE), such as the Laplace or biharmonic equation. Especially the latter, which shows good numerical performance for large displacements, is expensive. Moreover, from a continuous perspective, choosing the mesh motion technique is to a certain extent arbitrary and has no influence on the physically relevant quantities. Therefore, we consider approaches inspired by machine learning. We present a hybrid PDE-NN approach, where the neural network (NN) serves as parameterization of a coefficient in a second order nonlinear PDE. We ensure existence of solutions for the nonlinear PDE by the choice of the neural network architecture. Moreover, we propose a splitting of the monolithic FSI system into three smaller subsystems, in order to segregate the mesh motion. We assess the quality of the learned mesh motion technique by applying it to a FSI benchmark problem.

Keywords Fluid-structure interaction · shape optimization · neural networks · partial differential equations · hybrid PDE-NN · mesh moving techniques · data-driven approaches

1 Introduction

Extending boundary deformation onto the whole domain is a task that can be a crucial and limiting factor in applications. It appears in monolithic arbitrary Lagrangian-Eulerian (ALE) formulations of fluid-structure interaction (FSI) problems, e.g., [23, 19], and the method of mappings for partial differential equation (PDE) constrained shape optimization problems, e.g., [14, 17]. The task can be stated as follows. Let $\Omega \subset \mathbb{R}^d$, $d \in \{2, 3\}$, be a domain and $\partial\Omega$ be its boundary. Given a boundary displacement $g : \partial\Omega \rightarrow \mathbb{R}^d$, one needs to apply an extension operator to find a deformation field $u : \Omega \rightarrow \mathbb{R}^d$ such that $u|_{\partial\Omega} = g$ and $(\text{id} + u)(\Omega)$ is a well-defined (Lipschitz) domain. This imposes requirements on g and the extension operator. Among other things, $\text{id} + u : \Omega \rightarrow (\text{id} + u)(\Omega)$ needs to be bijective, which also implies that g has to be chosen appropriately (e.g. not leading to a self-intersecting boundary of Ω). For computational purposes, it is mandatory that for any fixed mesh that discretizes Ω the transformed mesh is non-degenerate. The task of finding a suitable extension operator is typically based on heuristic choices, and has no (from a continuous perspective) or little (from a numerical perspective) influence on the physical solution as long as it is ensured that it fulfills the above described requirements. At the same time, it is the limiting factor for numerical simulations as soon as these requirements are violated. In this work, we apply ideas from machine learning to find a suitable extension operator.

*Johannes Haubner acknowledges support from the Research Council of Norway, grant 300305. Miroslav Kuchta acknowledges support from the Research Council of Norway, grant 303362.

Several approaches to define the extension operator have been introduced in the literature. In [23], harmonic extension operators, a linear elastic and a biharmonic model have been compared in the context of monolithic ALE formulations of FSI problems. The harmonic extension operator is obtained by solving the PDE

$$-\Delta u = 0 \quad \text{in } \Omega, \quad u = g \quad \text{on } \partial\Omega. \quad (1)$$

The linear elastic model is given by

$$-\operatorname{div}(\eta_\lambda \operatorname{tr}(\epsilon)I + 2\eta_\mu \epsilon) = 0 \quad \text{in } \Omega, \quad u = g \quad \text{on } \partial\Omega, \quad (2)$$

with $\epsilon = \frac{1}{2}(\nabla u + \nabla u^\top)$ and scalar valued functions η_λ, η_μ that are chosen, e.g., mesh size dependent. In the context of shape optimization, [17] chooses $\eta_\lambda = 0$ and $\eta_\mu = \mu$, where μ solves the PDE

$$-\Delta \mu = 0 \quad \text{in } \Omega, \quad \mu = \mu_{\max} \quad \text{on } \Gamma, \quad \mu = \mu_{\min} \quad \text{on } \partial\Omega \setminus \Gamma, \quad (3)$$

for constants $\mu_{\max}, \mu_{\min} > 0$. The manually chosen boundary value allows to increase rigidity in areas where large deformations occur, e.g., around $\partial\Omega$. Finally, the biharmonic model given by

$$\Delta^2 u = 0 \quad \text{in } \Omega, \quad u = g, \quad \nabla u \cdot n = 0 \quad \text{on } \partial\Omega, \quad (4)$$

shows the best numerical behavior. However, it is the most expensive option since it requires either H^2 -conforming finite elements, or other techniques such as a mixed approach, cf. e.g. [23, Sec. 4.4.5], or weakly imposed continuity of the normal derivatives [6]. Recently, in the context of shape optimization, also different types of extension equations were used. Here, in contrast to fluid-structure interaction simulations, the choice of nonlinear extension operators is justified in many applications since solving governing time-dependent PDEs for the state equation is the computational bottleneck of the simulation. Differently from the fluid-structure interaction application, the choice of the extension operator can be part of the modeling and, e.g., used to define a shape metric based on the corresponding Steklov-Poincaré operator [18]. In [14], the p -Laplacian for $p \geq 2$ was introduced as an extension equation. For $1 < p < \infty$, the problem is given by

$$-\operatorname{div}(\|\nabla u\|^{p-2} \nabla u) = 0 \quad \text{in } \Omega, \quad u = g \quad \text{on } \partial\Omega, \quad (5)$$

where $\|\cdot\|$ denotes the Frobenius norm. The nonlinearity increases the rigidity for increasing deformation gradient.

Considering the above approaches, we observe that the harmonic extension operator and the p -Laplacian are special cases of the more general formulation

$$-\operatorname{div}(\bar{\alpha}(\theta, \xi, u, \nabla u) \nabla u) = 0 \quad \text{in } \Omega, \quad u = g \quad \text{on } \partial\Omega, \quad (6)$$

where $\bar{\alpha}$ is a scalar valued function, ξ denotes the coordinates and θ parameters (e.g., $\theta = p$, $\theta = \mu$). Here we shall parameterize $\bar{\alpha}$ by using a neural network and in turn θ represents the network's weights and biases. The choice of $\bar{\alpha}$ is made based on theoretical considerations such that existence of solutions of (6) is ensured. This requires a sophisticated choice of the architecture and the weights. We note that our approach is an instance of an hybrid PDE-NN model [13].

Incorporating prior knowledge to train neural networks is a common strategy. Features like periodicity, can be guaranteed in the network architectures by using a feature transformation, see e.g. [26]. Theoretical considerations and classical discretization schemes can be used as prior knowledge and be respected in the NN architecture. The choice in [16] is, e.g., based on theory of unsteady partial differential equations. On unstructured meshes, the connection between message-passing neural networks and classical discretization schemes is demonstrated in [11]. Physics-informed neural networks [15] incorporate knowledge or modeling assumptions on the physical model in the objective function. The hybrid PDE-NN approach proposed in [10, 25, 13] can itself be viewed as a (non-standard) neural network approach that learns a solution operator $g \mapsto u$ of (6) from data and involves a solve of a partial differential equation in the output layer, which makes evaluations expensive compared to standard neural network architectures. Learning partial differential equations from data is also addressed e.g. in [1, 3, 4].

In the scope of the work, for the sake of simplicity, we restrict ourselves to $\bar{\alpha}(\theta, \xi, u, \nabla u) = \alpha(\theta, \|\nabla u\|^2)$. We make a theoretically funded choice for the neural net, which serves as parameterization for $\bar{\alpha}$, such that existence of solutions of (6) is ensured. The choice of $\bar{\alpha}$ then allows us to prove well-posedness of the extension operator by applying ideas from the proof that the p -Laplace equations have unique solutions. Moreover, we follow a supervised learning approach that aims to find a neural network such that the solution of (6) is close to the solution of the biharmonic extension. Given boundary displacements g^i , $i \in \{1, \dots, N_d\}$, $N_d \in \mathbb{N}$, we search for weights θ such that

$$\frac{1}{N_d} \sum_{i=1}^{N_d} \|u^i - u_{ref}^i\|^2 \quad (7)$$

is minimized, where u^i solves (6) and u_{ref}^i the biharmonic equation for boundary conditions $g = g^i$. Moreover, $\|\cdot\|$ denotes an appropriate norm. We work with

$$\|\cdot\|^2 = \|\cdot\|_{L^2(\Omega)}^2 + \|\nabla \cdot\|_{L^2(\Omega)}^2. \quad (8)$$

The resulting extension equation is nonlinear. In order to make it suitable in the setting of the unsteady FSI equations, we follow a “lagging nonlinearity” approach, i.e. we consider the linear extension equation $-\operatorname{div}(\bar{\alpha}(\theta, \xi, \bar{u}, \nabla \bar{u}) \nabla u) = 0$ with \bar{u} being the deformation variable of the previous time-step in order to compute the new deformation field.

To assess the quality of the learned extension operator, we apply it to the FSI benchmark II [22]. More precisely, we do a comparison similar to [23, Fig. 6]. In order to be able to include different extension operators and assess their quality without having to modify the FSI system, we introduce a novel splitting scheme for the monolithic system. This splitting is, in particular, useful for ongoing research, where we test other methods that are not based on a hybrid PDE-NN approach.

We introduce the problem formulation and motivate the choice of $\bar{\alpha}$ in Section 2. Section 3 presents the splitting for the monolithic FSI formulation. Numerical results are present in Section 4.¹

2 Hybrid NN-PDE Approach

In order to find the extension operator via (6), we formulate an optimization problem to find $\bar{\alpha}$:

$$\begin{aligned} \min_{\theta \in \Theta, u \in W} \quad & \frac{1}{N_d} \sum_{i=1}^{N_d} \|u^i - u_{ref}^i\|^2 + \lambda \mathcal{R}(\theta) \\ \text{s.t.} \quad & -\operatorname{div}(\bar{\alpha}(\theta, \xi, u^i, \nabla u^i)(\nabla u^i)) = 0 \quad \text{in } \Omega, \\ & u^i = g^i \quad \text{on } \partial\Omega, \end{aligned} \quad (9)$$

where $\lambda > 0$ denotes a regularization parameter, $\mathcal{R}(\theta)$ a regularization term, Θ and W closed subsets of suitable Banach spaces, and $\|\cdot\|$ is defined in (8). In order for the optimization problem to be well-defined, we have to choose $\bar{\alpha}$ in a way such that the PDE constraint in (9) is solvable for all admissible $\theta \in \Theta$. This requires a suitable choice of Θ and $\bar{\alpha}$, which we address in Section 2.2. We model $\bar{\alpha}$ via a neural net. Hence, we are in the setting of hybrid PDE-NN models [13].

2.1 Choice of $\bar{\alpha}$

The partial differential equation (6) is not necessarily solvable if we choose $\bar{\alpha}(\theta, \xi, u, \nabla u)$ arbitrarily. In order to find conditions for $\bar{\alpha}$ under which (6) can be ensured to be uniquely solvable, we take inspiration from the p -Laplace equations. The weak formulation of the p -Laplace equations, $p > 1$, can be viewed as the optimality conditions of the optimization problem

$$\min_{u \in W} \int_{\Omega} \|\nabla u\|^p d\xi. \quad (10)$$

Since (10) is a convex optimization problem with strictly convex objective, (10) has a unique solution. More precisely, we have the following result.

Lemma 1 (see [12, Thm. 2.16]). *Let Ω be a bounded Lipschitz domain, $p \geq 2$, $g \in W^{1,p}(\Omega)$. Moreover, let*

$$W = \{u \in W^{1,p}(\Omega) : u|_{\partial\Omega} = g|_{\partial\Omega}\}.$$

Then, there exists a unique minimizer of the optimization problem (10) and the solution of the optimization problem is characterized by

$$(\|\nabla u\|^{p-2} \nabla u, \nabla \eta)_{L^2(\Omega)} = 0 \quad \forall \eta \in W_0^{1,p}(\Omega).$$

We prove a similar result for a more general class of PDEs. Hence, we consider a mapping $\Lambda : \mathbb{R} \rightarrow \mathbb{R}$ and the optimization problem

$$\min_{u \in W} \int_{\Omega} \Lambda(\|\nabla u\|^2) d\xi \quad (11)$$

¹The code is available at <https://github.com/JohannesHaubner/LearnExt>.

and work with

$$\alpha(\|\nabla u\|^2) = 2\Lambda'(\|\nabla u\|^2). \quad (12)$$

Lemma 2. *Let Ω be a bounded Lipschitz domain and g, W be defined as in Lemma 1. Let $\Lambda : \mathbb{R} \rightarrow \mathbb{R}$ be such that*

- Λ is convex,
- Λ is strictly increasing,
- Λ is continuously differentiable,
- there exist $a, b, d > 0, c \in \mathbb{R}$ and $p > 2$ (or $p = 2$ and Λ being affine) such that

$$|\Lambda(t)| \leq a + bt^{\frac{p}{2}}, \quad (13)$$

and

$$|\Lambda'(t)| \leq c + dt^{\frac{p}{p-2}}, \quad (14)$$

and α be defined by (12). Then the mapping

$$F : W \rightarrow \mathbb{R}, \quad u \mapsto \int_{\Omega} \Lambda(\|\nabla u\|^2) d\xi, \quad (15)$$

is convex, continuous and Fréchet differentiable with derivative

$$F'(u) : W_0^{1,p}(\Omega) \rightarrow \mathbb{R}, \quad h_u \mapsto \int_{\Omega} 2\alpha(\|\nabla u\|^2)(\nabla u : \nabla h_u) d\xi. \quad (16)$$

Proof. In order to show continuity and differentiability of F , we rewrite

$$F(u) = f_3 \circ f_2 \circ f_1(u),$$

where

$$\begin{aligned} f_1 : W^{1,p}(\Omega)^d &\rightarrow L^p(\Omega)^{d \times d}, \quad v \mapsto \nabla v, \\ f_2 : L^p(\Omega)^{d \times d} &\rightarrow L^{\frac{p}{2}}(\Omega), \quad B \mapsto \|B\|^2, \\ f_3 : L^{\frac{p}{2}}(\Omega) &\rightarrow \mathbb{R}, \quad \beta \mapsto \int_{\Omega} \Lambda(\beta) d\xi. \end{aligned} \quad (17)$$

Since f_1 is linear, f_2 is strictly convex and Λ is strictly increasing, F is convex. Due to [21, Sec. 4.3.3] we know that the superposition operator f_2 is continuous and continuously differentiable with derivative $f_2'(B) : L^p(\Omega)^{d \times d} \rightarrow L^{\frac{p}{2}}(\Omega)$, $h_B \mapsto 2(B : h_B)$, where $B : h_B := \sum_{i,j} B_{ij}(h_B)_{ij}$. Due to (13) and (14), we further obtain continuity and differentiability of f_3 with derivative $f_3'(\beta) : L^{\frac{p}{2}}(\Omega) \rightarrow \mathbb{R}$, $h_\beta \mapsto \int_{\Omega} \Lambda'(\beta) h_\beta d\xi$. Due to linearity and boundedness, f_1 is continuous and differentiable with $f_1'(v) : W^{1,p}(\Omega)^d \rightarrow L^p(\Omega)^{d \times d}$, $h_v \mapsto \nabla h_v$. Hence, by applying the chainrule we obtain continuity and differentiability of $F : W^{1,p}(\Omega)^d \rightarrow \mathbb{R}$ with derivative $F'(v)(h_v) = \int_{\Omega} 2\Lambda'(\|\nabla v\|^2)(\nabla v : \nabla h_v) d\xi$. Since W is a closed, affine linear subspace of $W^{1,p}(\Omega)^d$, this concludes the proof. \square

Lemma 3. *Let the prerequisites of Lemma 2 be fulfilled. Assume further that there exist $e, f > 0$, such that*

$$|\Lambda(t)| \geq e + ft^{\frac{p}{2}}. \quad (18)$$

Moreover, let $g \in W^{1,p}(\Omega)$ and

$$W = \{u \in W^{1,p}(\Omega) : u|_{\partial\Omega} = g|_{\partial\Omega}\}.$$

Then, there exists a unique minimizer of the optimization problem (10) and the solution of the optimization problem is characterized by

$$(\alpha(\|\nabla u\|^2)\nabla u, \nabla \eta)_{L^2(\Omega)} = 0 \quad \forall \eta \in W_0^{1,p}(\Omega). \quad (19)$$

Proof. The proof follows the line of argumentation of [12, Thm. 2.16]. Assume $u_1, u_2 \in W$ are solutions of (11). Since Λ is convex and strictly increasing and $\nabla u \mapsto \|\nabla u\|^2$ is strictly convex, we know that $\nabla u \mapsto \Lambda(\|\nabla u\|^2)$ is strictly convex. Hence, we know that $\nabla u_1 = \nabla u_2$. Therefore, $u_1 = u_2 + C$ for a constant $C > 0$. Due to $(u_1 - u_2)|_{\partial\Omega} = 0$, $C = 0$. This shows uniqueness of minimizers for (11).

In the following, we show existence of solutions. By the continuity of F shown in Lemma 2, we have

$$I_0 := \inf_{v \in W} \int_{\Omega} \Lambda(\|\nabla v\|^2) d\xi \leq \int_{\Omega} \Lambda(\|\nabla g\|^2) d\xi < \infty. \quad (20)$$

Therefore, we can choose a sequence $(v_j)_{j \in \mathbb{N}} \subset W$ such that $\int_{\Omega} \Lambda(\|\nabla v_j\|^2) d\xi < I_0 + \frac{1}{j}$ for all $j \in \mathbb{N}$. Due to (18), we know that $\|\nabla v_j\|_{L^p(\Omega)}$ is bounded. Since, by the Poincaré inequality, there exists a constant $C > 0$ such that $\|w\|_{L^p(\Omega)} \leq C \|\nabla w\|_{L^p(\Omega)}$ for all $w \in W_0^{1,p}(\Omega)$, we know that $\|v_j - g\|_{L^p(\Omega)} \leq C \|\nabla(v_j - g)\|_{L^p(\Omega)}$ for all $j \in \mathbb{N}$. This implies boundedness of the sequence $(\|v_j\|_{W^{1,p}(\Omega)})_{j \in \mathbb{N}}$. Hence, there exists a weakly convergent subsequence $(v_j)_{j \in J \subset \mathbb{N}}$ and $v \in W$ such that $v_j \rightharpoonup v$ weakly in $W^{1,p}(\Omega)$ for $J \ni j \rightarrow \infty$. Since, by Lemma 2, $F : W \rightarrow \mathbb{R}$ is convex and continuous, it is weakly lower semicontinuous. Therefore, $F(v) \leq \liminf_{J \ni j \rightarrow \infty} F(v_j) = I_0$ and v is the unique minimizer of (11). The first order necessary optimality conditions for the unconstrained optimization problem then yield (19). \square

2.2 Choice of the neural network

We do a slight abuse of notation and write $\alpha(\theta, s)$ instead of $\alpha(s)$, as well as $\Lambda(\theta, s)$ instead of $\Lambda(s)$, in order to stress that our choices of α and Λ depend on the weights and biases θ of a neural net. By the considerations of the previous section, we choose

$$\bar{\alpha}(\theta, \xi, u, \nabla u) = \alpha(\theta, \|\nabla u\|^2) = 2 \frac{d}{ds} \Lambda(\theta, \|\nabla u\|^2),$$

where $\Lambda : \Theta \times \mathbb{R} \rightarrow \mathbb{R}$ fulfills the requirements of (19). More precisely, we work with

$$\alpha(\theta, s) := 1 + (s - \eta_1)_{+, \epsilon} \frac{d}{ds} \tilde{\Lambda}(\theta, s) + (s - \eta_2)_{+, \epsilon}, \quad (21)$$

where $\eta_1 > 0$, $\eta_2 \gg \eta_1$, $\epsilon > 0$, $(\cdot)_{+, \epsilon}$ denotes a monotonically increasing, smooth approximation of the $\max(\cdot, 0)$ function and $\tilde{\Lambda}(\theta, s)$ denotes a continuously differentiable, monotonically increasing, nonnegative Input Output Convex Neural Network [2, 20] that fulfills $\tilde{\Lambda}(\theta, s) = \mathcal{O}(s)$ for $s \rightarrow \infty$. The last summand is not realized in the numerics and only needed if the second summand is zero.

The reason why we choose this specific form of α is due to the fact that we want to keep the linearity of the extension operator close to the identity.

The Λ associated to (21) fulfills the properties of Lemma 3:

- Since $s \mapsto \tilde{\Lambda}(\theta, s)$ is convex and the mappings $s \mapsto (s - \eta_1)_{+, \epsilon}$ and $s \mapsto (s - \eta_2)_{+, \epsilon}$ are monotonically increasing, $\frac{d}{ds} \alpha(\theta, s)$ is non-negative and Λ is convex.
- Since $s \rightarrow \tilde{\Lambda}(\theta, s)$ is monotonically increasing, $\frac{d}{ds} \tilde{\Lambda}(\theta, s) \geq 0$. Therefore, $\alpha(\theta, s) \geq 1$ and Λ is strictly increasing.
- Continuous differentiability of Λ follows from α being a composition of continuous functions.
- The lower and upper bound estimates (13), (14) and (18) hold for $p = 4$.

In order to fulfill the requirements we ensure that the weights of $\tilde{\Lambda}$ are nonnegative (we realize this by using squared weights).

Let σ denote a continuously differentiable activation function with derivative σ' . We work with the standard softmax function $\sigma(x) = \ln(1 + e^x)$, with its derivative, the sigmoid function, $\sigma'(x) = \frac{e^x}{1+e^x} = \frac{1}{1+e^{-x}}$.

The neural network $\tilde{\Lambda}(\theta, s) = x_{k+1}$ is given by the recursion

$$\begin{aligned} x_{k+1} &= W_k x_k + b_k, \\ x_{\ell+1} &= \sigma(W_{\ell} x_{\ell} + b_{\ell}), \quad \text{for } \ell \in \{0, \dots, k-1\} \\ x_0 &= s, \end{aligned}$$

with $((W_0, b_0), (W_1, b_1), \dots, (W_k, b_k)) = \psi(\theta)$, $\theta = ((W_0^\theta, b_0^\theta), (W_1^\theta, b_1^\theta), \dots, (W_k^\theta, b_k^\theta))$,

$$\psi : ((W_0^\theta, b_0^\theta), (W_1^\theta, b_1^\theta), \dots, (W_k^\theta, b_k^\theta)) \mapsto ((s[W_0^\theta], b_0^\theta), (s[W_1^\theta], b_1^\theta), \dots, (s[W_k^\theta], b_k^\theta)),$$

where $s : t \mapsto t^2$, and we use the notation in [9] to denote by $s[\cdot]$ the entrywise application of s to a matrix \cdot . Moreover, since it is not present in the derivative of the network, we choose the bias in the output layer as $b_k^\theta = 0$, where k is the depth of the neural network. Its derivative is therefore given by $\frac{d}{ds} \tilde{\Lambda}(\theta, s) = y_{k+1}$, where

$$\begin{aligned} y_{k+1} &= W_k y_k, \\ (y_{\ell+1})_i &= \sum_j \sigma'(W_\ell x_\ell + b_\ell)_i (W_\ell)_{i,j} (y_\ell)_j, \quad \text{for } \ell \in \{0, \dots, k-1\}, \\ x_\ell &= \sigma(W_{\ell-1} x_{\ell-1} + b_{\ell-1}), \quad \text{for } \ell \in \{0, \dots, k-1\}, \\ x_0 &= s, \quad y_0 = 1. \end{aligned}$$

Hence, motivated by theoretical considerations, we work with a non-standard neural network architecture.

3 FSI model

In order to test the learned extension operator and compare it with respect to extension quality, we apply it to the FSI benchmark II. We consider the coupling of the Navier-Stokes equations with St. Venant Kirchhoff type material and choose a monolithic ALE setting formulated on a fixed reference domain.

For the sake of convenience and brevity, we present the PDE system with a harmonic extension equation for the fluid displacement - other extension equations are more meaningful for large displacements and can be straightforwardly included into the system of equations [23, 7] as long as they can be represented as PDEs. The FSI model reads as follows.

$$\begin{aligned} J\rho_f \partial_t v_f + J\rho_f ((F^{-1}(-\partial_t w_f)) \cdot \nabla) v_f - \operatorname{div}(J\sigma_f F^{-\top}) &= J\rho_f f & \text{on } \Omega_f \times (0, T), \\ \operatorname{div}(JF^{-1}v_f) &= 0 & \text{on } \Omega_f \times (0, T), \\ v_f &= v_{fD} & \text{on } \Gamma_f \times (0, T), \\ v_f(0) &= 0 & \text{on } \Omega_f, \\ \rho_s \partial_t v_s - \operatorname{div}(J\sigma_s F^{-\top}) &= \rho_s f_s & \text{on } \Omega_s \times (0, T), \\ \rho_s \partial_t w_s - \rho_s v_s &= 0 & \text{on } \Omega_s \times (0, T), \\ w_s(0) &= 0 & \text{on } \Omega_s, \\ v_s(0) &= 0 & \text{on } \Omega_s, \\ -\Delta w_f &= 0 & \text{on } \Omega_f \times (0, T), \\ w_f &= w_{fD} & \text{on } \Gamma_f \times (0, T), \\ \nabla w_f \cdot n &= 0 & \text{on } \Gamma_f \times (0, T), \\ \partial_t w_s &= v_s = v_f & \text{on } \Gamma_i \times (0, T), \\ -J\sigma_f F^{-\top} n_f &= J\sigma_s F^{-\top} n_s & \text{on } \Gamma_i \times (0, T), \\ w_f &= w_s & \text{on } \Gamma_i \times (0, T), \end{aligned}$$

where

$$\begin{aligned} \sigma_f(F) &= \rho_f \nu_f (Dv_f F^{-1} + F^{-\top} Dv_f^\top) - p_f \mathbf{I}, \\ F &= \mathbf{I} + Dw_s, \quad J(F) = \det(F), \quad E(F) = \frac{1}{2}(F^\top F - \mathbf{I}) \end{aligned}$$

and

$$\sigma_s(F) = J(F)^{-1} F (\mu_s (F^\top F - \mathbf{I}) + \lambda_s \operatorname{tr}(E(F)) \mathbf{I}) F^\top$$

for St. Venant Kirchhoff type material. Whenever it is clear from the context we write J , E , σ_f , σ_s instead of $J(F)$, $E(F)$, $\sigma_f(F)$, $\sigma_s(F)$.

$D \cdot$ denotes the Jacobian of \cdot . We have some compatibility conditions: $v_{fD} = \partial_t w_{fD}$, $v_{fD}(0) = 0$. Let

$$\begin{aligned} V &\subset \{v \in H^1(\Omega)^d : v|_{\Gamma_f} = v_{fD}\}, \\ V_0 &\subset \{v \in H^1(\Omega)^d : v|_{\Gamma_f} = 0\}, \\ W &\subset \{v \in H^1(\Omega)^d : w|_{\Gamma_f} = w_{fD}\}, \\ W_0 &\subset \{v \in L^2(\Omega) : v|_{\Omega_f} \in H_0^1(\Omega_f)^d, v|_{\Omega_s} \in H^1(\Omega_s)^d\}, \\ P &\subset \{p \in L^2(\Omega_f) : \int_{\Omega_f} p d\xi = 0\}. \end{aligned}$$

The weak formulation is given by: Find $(v, p, w) \in V \times P \times W$ such that

$$\begin{aligned} \mathcal{A}(v, p, w)(\psi^v, \psi^p, \psi^w) &= (J\rho_f \partial_t v, \psi^v)_{\Omega_f} + (J\rho_f((F^{-1}(-\partial_t w)) \cdot \nabla)v, \psi^v)_{\Omega_f} + (J\sigma_f F^{-\top}, D\psi^v)_{\Omega_f} \\ &\quad - (J\rho_f f, \psi^v)_{\Omega_f} + (\rho_s \partial_t v, \psi^v)_{\Omega_s} + (J\sigma_s F^{-\top}, D\psi^v)_{\Omega_s} + (\rho_s(\partial_t w - v), \psi^w)_{\Omega_s} \\ &\quad + \alpha_w(Dw, D\psi^w)_{\Omega_f} + (\operatorname{div}(JF^{-1}v), \psi^p)_{\Omega_f} = 0 \end{aligned} \quad (22)$$

for all $(\psi^v, \psi^p, \psi^w) \in V_0 \times P \times W_0$.

3.1 Splitting the FSI problem into smaller subproblems

We have to solve the nonlinear system of equations $\mathcal{A}(v, p, w) = 0$. In order to simplify the use of arbitrary extension operators, we propose a splitting scheme that handles the extension in a separate step. To do so, we build on ideas and techniques that are also present in, e.g., [5, 24].

The method proposed in [5] substitutes the condition $\partial_t w_s = v_s$, i.e. $w_s(t + \Delta t) = w_s(t) + \int_t^{t+\Delta t} v_s(\xi) d\xi$, into σ_s . It then consists of Gauss-Seidel sweeps through the whole nonlinear system and is motivated as an inexact Newton method.

We motivate a similar procedure, use the reasoning of [5] to reduce the system but combine it with another idea. After transformation to the physical domain, the choice of w_f in the interior of Ω_f does not affect the result of the fluid solution (as long as it is ensured that the corresponding transformation is bi-Lipschitz). Therefore, in the first step, we use $w(t + \Delta t) = \tilde{w}(t) + \int_0^{\Delta t} v(t + s) ds$, where $\tilde{w}(t)$ denotes a deformation field at timepoint t . After having computed $v(t + \Delta t)$ and $p(t + \Delta t)$, we compute $w|_{\Omega_s}(t + \Delta t)$ and $\tilde{w}(t + \Delta t)$ by applying an extension operator of the solid displacement onto the fluid domain. In this way, we solve for (v, p) and \tilde{w} separately without doing an approximation. Then, we need to recompute (v, p) for the modified deformation field \tilde{w} (which replaces w for the time-stepping). Thus, the procedure requires to solve the fluid system twice.

More precisely, assume we know the states \tilde{w}, v, p at the time step t . In order to get the states at time step $t + \Delta t$ we have to solve three systems of equations. For the case of using an harmonic extension operator the procedure is given as follows.

First system. Let $F(t + \delta t) = I + D(\tilde{w} + \int_t^{t+\delta t} v(\xi) d\xi)$, $J = \det(F)$ and get $v(t + \delta t)$, $p(t + \delta t)$ for any $\delta t > 0$ as the solution of

$$\begin{aligned} &(J\rho_f \partial_t v, \psi^v)_{\Omega_f} + (J\sigma_f F^{-\top}, D\psi^v)_{\Omega_f} \\ &\quad - (J\rho_f f, \psi^v)_{\Omega_f} + (\rho_s \partial_t v, \psi^v)_{\Omega_s} + (J\sigma_s F^{-\top}, D\psi^v)_{\Omega_s} \\ &\quad + (\operatorname{div}(JF^{-1}v), \psi^p)_{\Omega_f} = 0, \end{aligned} \quad (23)$$

with $\sigma_f = \sigma_f(F)$ and $\sigma_s = \sigma_s(F)$.

Second system. Given the solution of the first system we consider the solution of

$$(\rho_s(\partial_t w - v), \psi_s^w)_{\Omega_s} + \alpha_w(Dw, D\psi_f^w)_{\Omega_f} = 0, \quad (24)$$

where we impose the Dirichlet boundary conditions $w|_{\partial\Omega_f} = (\tilde{w} + \int_t^{t+\delta t} v(\xi) d\xi)|_{\partial\Omega_f}$. The solution of this system is used to update \tilde{w} . (Here, we use the subscripts \cdot_f and \cdot_s in order to clarify that these two equations are solved independently.) It is straightforward to replace the harmonic extension with an arbitrary extension

operator that extends the boundary displacement to the interior of the domain, e.g., also those that are not defined via the solution of a PDE.

Third system. Given \tilde{w} we obtain the updated v, p as the solution of

$$\begin{aligned} & (J\rho_f\partial_tv, \psi^v)_{\Omega_f} + (J\rho_f((F^{-1}(v - \partial_tw)) \cdot \nabla)v, \psi^v)_{\Omega_f} + (J\sigma_f F^{-\top}, D\psi^v)_{\Omega_f} \\ & - (J\rho_f f, \psi^v)_{\Omega_f} + (\rho_s\partial_tv, \psi^v)_{\Omega_s} + (J\sigma_s F^{-\top}, D\psi^v)_{\Omega_s} \\ & + (\text{div}(JF^{-1}v), \psi^p)_{\Omega_f} = 0. \end{aligned} \quad (25)$$

where $F = I + D(\tilde{w})$, $J = \det(F)$, $\sigma_f = \sigma_f(F)$ and $\sigma_s = \sigma_s(F_s)$ with $F_s(t + \delta t) = \tilde{w} + \int_t^{t+\delta t} v(\xi)d\xi$.

3.2 Discretization

The discretization is done as in [23, 5, 7]. We choose the lowest-order Taylor-Hood finite elements for the velocity and pressure. The deformation is discretized using piecewise quadratic continuous finite elements. We further choose a shifted Crank-Nicolson scheme for performing the time-stepping. The pressure term and the incompressibility condition are handled implicitly. In the first summand of the weak form, J is replaced by a J_θ , which is a convex combination of the determinant of the deformation gradient of the previous and current time step.

The time-step size is iteratively adapted. We choose a time-step-size range $[\Delta t_{min}, \Delta t_{max}]$ and start with time-steps of size $\Delta t = \Delta t_{max}$. If the systems with the maximal time-step get unsolvable, we choose $\Delta t = \max(\Delta t_{min}, \frac{1}{2}\Delta t)$. This is repeated until we obtain solvability or reach Δt_{min} . If the system is not solvable for $\Delta t = \Delta t_{min}$, we stop. After each successful step we adapt the time-step by setting $\Delta t = \min(2\Delta t, \Delta t_{max})$.

4 Numerical Results

In order to validate the splitting of the FSI system in Section 3.1, we apply it to the FSI benchmark II [22] and plot the displacement of the tip of the flap in Figure 1, compare e.g. [22, p. 256] or [7, Fig. 5.6]. We test the harmonic extension, the biharmonic extension and an incremental version of the harmonic extension where the extension is performed on the deformed domain of the previous timestep and only the change of the displacement is extended harmonically, see [19]. Moreover, Figure 1 shows the chosen time-step size and the minimal determinant value of the deformation gradient. The simulation of the standard and incremental (see [19]) harmonic extension break if the deformation gradient for the next time-step is close to being non-invertible. Therefore, with these approaches, it is not possible to simulate the whole time interval of 15s.

4.1 Generation of Training Data for hybrid PDE-NN model

To generate training data, we run the FSI benchmark II with the biharmonic extension and a time-step size of 0.0025, and save the deformations for every time step in $(15s, 17s]$, i.e., we generate $N_d = 800$ data points.

Remark 1. *This procedure only makes sense if the FSI problem is solved several times as it is the case, e.g., if the FSI equations are the governing equations of a PDE constrained optimization problem. Moreover, since it is not necessary that the test data is physically realistic, the test set can also be artificially generated. Instead of solving the biharmonic equations and using this as a reference value, also unsupervised learning approaches*

$$\begin{aligned} & \min_{\theta \in \Theta, u \in W} \frac{1}{N_d} \sum_{i=1}^{N_d} \mathcal{J}(u^i) + \lambda \mathcal{R}(\theta) \\ & \text{s.t. } u^i = \text{Ext}_\theta(g^i) \quad \text{for } i \in \{1, \dots, N_d\} \end{aligned}$$

can be considered, where Ext_θ denotes an extension operator that depends on the parameters θ and \mathcal{J} denotes a quality measure for the deformed mesh. For example, one can choose \mathcal{J} such that the determinant of the transformation gradient is bounded away from 0, see [8]. This, however, is left for future research.

4.2 Hybrid PDE-NN Approach

In order to reduce the computational burden, we only take every N th training data point into account and work with $N = 40$. Every objective function evaluation requires the solution of $\lfloor \frac{N_d}{N} \rfloor$ nonlinear PDEs (which

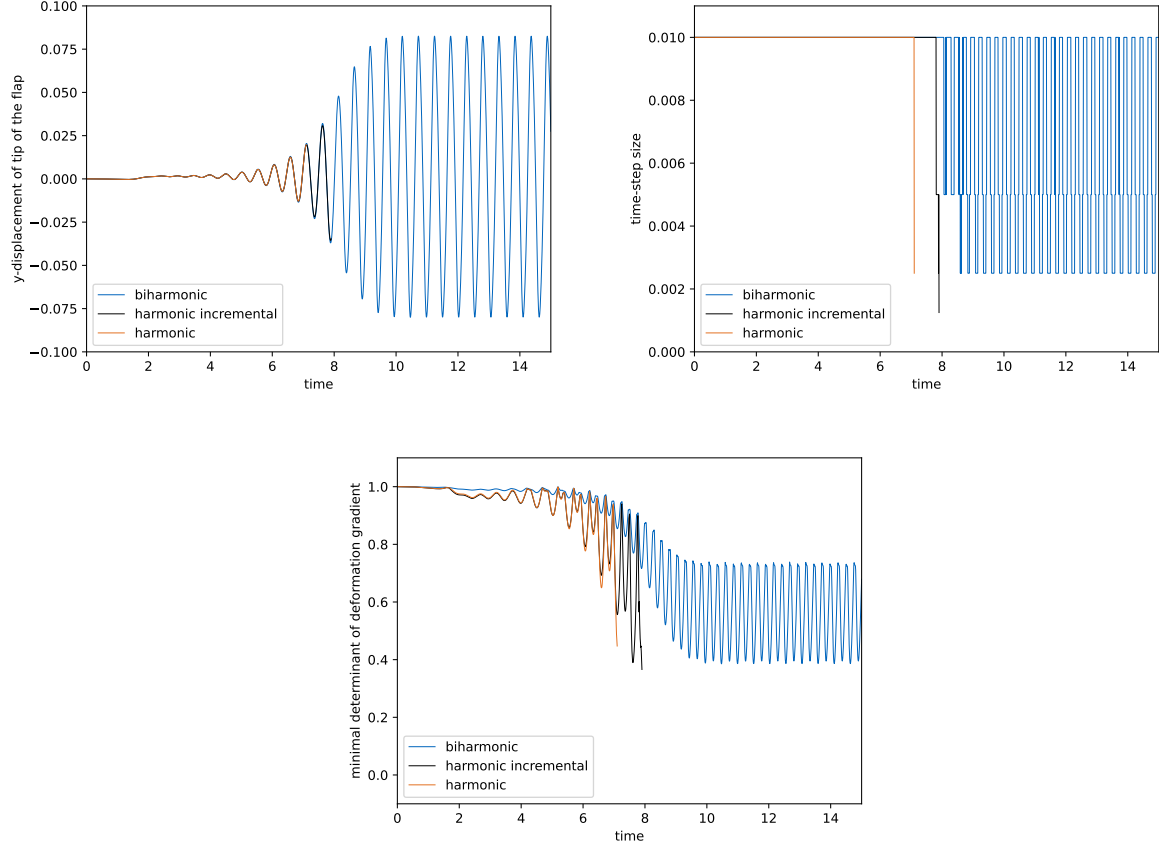


Figure 1: Numerical results for harmonic and biharmonic extension

could potentially be done fully parallel). In our numerical realization we do not use regularization, i.e., we work with $\lambda = 0$.

We choose α to be a neural network with two hidden layers of dimension 5 with bias on the two hidden layers. Let θ_{opt} denote the approximate solution of the optimization problem (9) that we obtain if we apply an L-BFGS method with at maximum 100 iterations. Figure 2 visualizes a neural network for $\theta = \theta_{opt}$ that we obtained by training. In our numerical experiments $\|\nabla u\|^2$ reaches values up to around 0.6 for the nonlinear learned extension operator applied to the FSI benchmark II.

We consider different strategies and show the numerical results in Figure 3 where we choose $\Delta t_{max} = 0.01$ and $\Delta t_{min} = \frac{1}{128} \Delta t_{max}$:

- **Strategy 1:** First we try the learned nonlinear extension operator, i.e., we solve (6) with $\bar{\alpha}$ defined by (21) and $\theta = \theta_{opt}$. This strategy does not fail due to mesh degeneration. However, it requires several Newton-steps for large displacements.
- **Strategy 2:** In order to avoid the nonlinearity, we consider a strategy that uses a linear version of the extension operator. Working with a “lagging nonlinearity”, i.e., solving (6) with $\bar{\alpha}$ defined by (21) being approximated by

$$\bar{\alpha}(\theta_{opt}, \xi, u, \nabla u) \approx \alpha(\theta_{opt}, \|\nabla u_{old}\|^2), \quad (26)$$

where u_{old} denotes the displacement of the previous time-step shows unsatisfactory numerical behaviour. Therefore, we combine it with the idea of using incremental versions for extension operators, see [19]. We present results for the incremental “lagging nonlinearity” strategy, where we

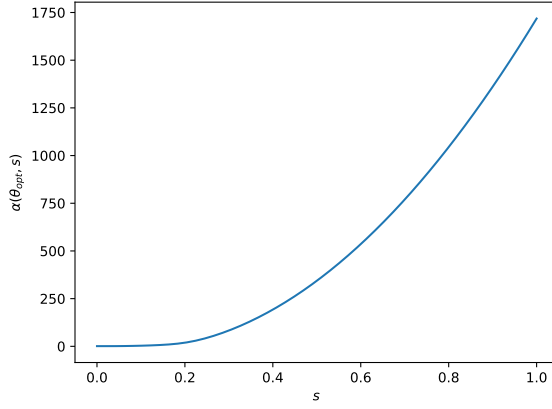


Figure 2: Visualization of learned neural net

solve

$$\begin{aligned} -\operatorname{div}(\alpha(\theta_{opt}, \|\nabla u_{old}\|^2) \nabla u_{\Delta}) &= 0 \quad \text{in } (\operatorname{id} + u_{old})(\Omega), \\ u_{\Delta} &= g - g_{old} \quad \text{on } \partial((\operatorname{id} + u_{old})(\Omega)), \end{aligned}$$

and use the update

$$u = u_{old} + u_{\Delta} \circ (\operatorname{id} + u_{old})^{-1}.$$

This strategy is successful even for the largest appearing displacements. However, the mesh quality decreases during the periodic oscillations and it is not possible to simulate the whole 15 seconds.

- **Strategy 3:** In order to counteract the decreasing mesh quality that occurs with the second strategy during the oscillations, we consider a third strategy that combines strategies 1 and 2. If the displacement of the tip of the flap is below a certain threshold (we use 0.005), we work with strategy 1, otherwise we choose strategy 2. This approach allows to simulate the whole 15 seconds and the mesh quality stays stable during the oscillations. Moreover, the nonlinear extension equation of strategy 1 just needs to be evaluated for few time-steps and in a regime with small deformations at the tip.

5 Conclusion

We presented a hybrid PDE-NN approach to learn a nonlinear second order partial differential equation. It approximates the solution of the biharmonic equation. We demonstrated that the learned equation has the potential to serve as mesh motion technique for FSI simulations and for shape optimization via the method of mappings. So far, we considered a supervised learning approach. For future work, it is also interesting to consider unsupervised approaches, where one tries to minimize a measure for the quality of the deformed mesh. Moreover, we applied an approach that requires the solution of a partial differential equation. Considering approaches that do not require the PDE solve is another task that we want to address in future research.

References

- [1] C. AARSET, M. HOLLER, AND T. T. N. NGUYEN, *Learning-informed parameter identification in nonlinear time-dependent PDEs*, 2022, <https://arxiv.org/abs/arXiv:2202.10915>.
- [2] B. AMOS, L. XU, AND J. Z. KOLTER, *Input convex neural networks*, in International Conference on Machine Learning, PMLR, 2017, pp. 146–155.
- [3] G. DONG, M. HINTERMUELLER, AND K. PAPAFITSOROS, *Optimization with learning-informed differential equation constraints and its applications*, 2020, <https://arxiv.org/abs/arXiv:2008.10893>.

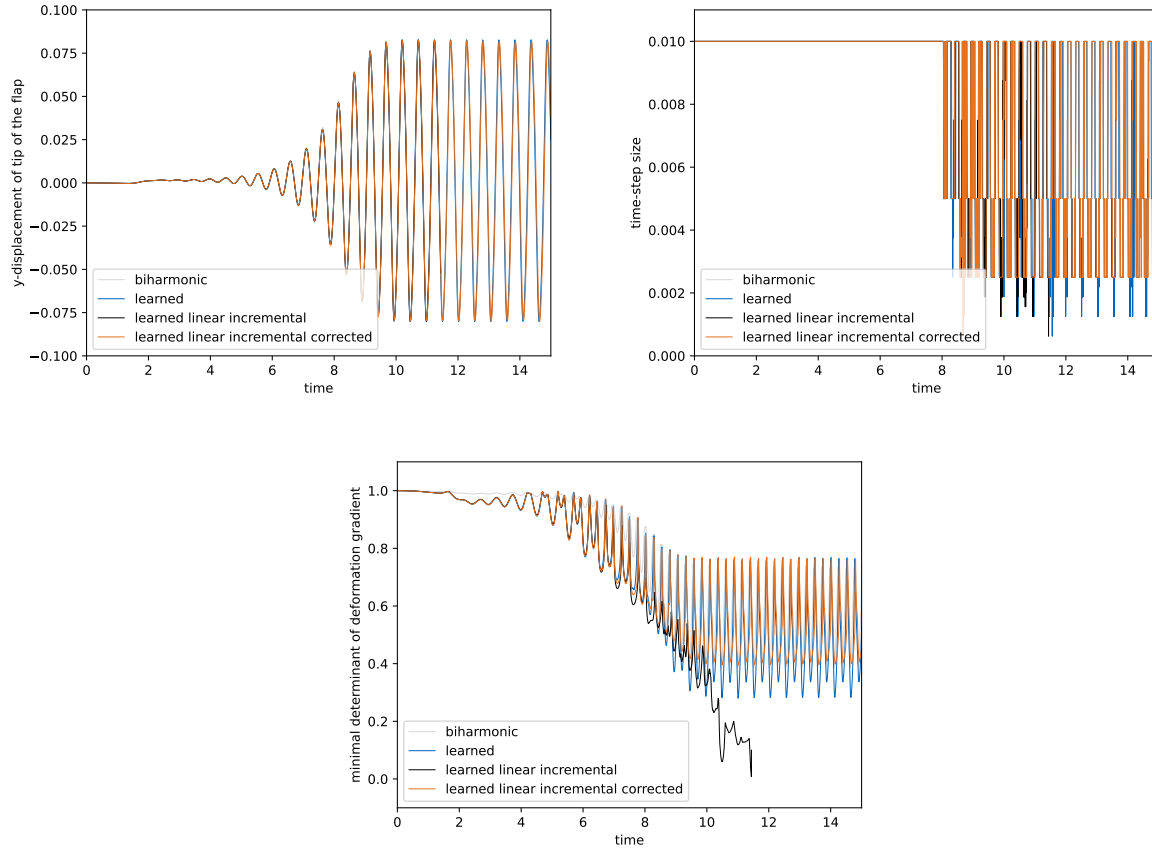


Figure 3: Numerical results for hybrid PDE-NN approach

- [4] G. DONG, M. HINTERMÜLLER, K. PAPAFITSOROS, AND K. VÖLKNER, *First-order conditions for the optimal control of learning-informed nonsmooth PDEs*, 2022, <https://arxiv.org/abs/arXiv:2206.00297>.
- [5] L. FAILER AND T. RICHTER, *A parallel Newton multigrid framework for monolithic fluid-structure interactions*, Journal of Scientific Computing, 82 (2020), pp. 1–27.
- [6] E. H. GEORGOULIS AND P. HOUSTON, *Discontinuous Galerkin methods for the biharmonic problem*, IMA journal of numerical analysis, 29 (2009), pp. 573–594.
- [7] J. HAUBNER, *Shape Optimization for Fluid-Structure Interaction*, Dissertation, Technische Universität München, München, 2020.
- [8] J. HAUBNER, M. SIEBENBORN, AND M. ULBRICH, *A continuous perspective on shape optimization via domain transformations*, SIAM Journal on Scientific Computing, 43 (2021), pp. A1997–A2018, <https://doi.org/10.1137/20m1332050>, <https://doi.org/10.1137/20m1332050>.
- [9] F. HIAI, *Monotonicity for entrywise functions of matrices*, Linear algebra and its applications, 431 (2009), pp. 1125–1146.
- [10] M. INNES, A. EDELMAN, K. FISCHER, C. RACKAUCKAS, E. SABA, V. B. SHAH, AND W. TEBBUTT, *A differentiable programming system to bridge machine learning and scientific computing*, arXiv preprint arXiv:1907.07587, (2019).
- [11] M. LIENEN AND S. GÜNNEMANN, *Learning the dynamics of physical systems from sparse observations with finite element networks*, arXiv preprint arXiv:2203.08852, (2022).
- [12] P. LINDQVIST, *Notes on the p -Laplace equation*, no. 161, University of Jyväskylä, 2017.

- [13] S. K. MITUSCH, S. W. FUNKE, AND M. KUCHTA, *Hybrid FEM-NN models: Combining artificial neural networks with the finite element method*, Journal of Computational Physics, 446 (2021), p. 110651, <https://doi.org/10.1016/j.jcp.2021.110651>, <https://doi.org/10.1016/j.jcp.2021.110651>.
- [14] P. M. MÜLLER, N. KÜHL, M. SIEBENBORN, K. DECKELNICK, M. HINZE, AND T. RUNG, *A novel p-harmonic descent approach applied to fluid dynamic shape optimization*, arXiv preprint arXiv:2103.14735, (2021).
- [15] M. RAISSI, P. PERDIKARIS, AND G. E. KARNIADAKIS, *Physics-informed neural networks: A deep learning framework for solving forward and inverse problems involving nonlinear partial differential equations*, Journal of Computational physics, 378 (2019), pp. 686–707.
- [16] L. RUTHOTTO AND E. HABER, *Deep neural networks motivated by partial differential equations*, Journal of Mathematical Imaging and Vision, 62 (2020), pp. 352–364.
- [17] V. SCHULZ AND M. SIEBENBORN, *Computational comparison of surface metrics for PDE constrained shape optimization*, Computational Methods in Applied Mathematics, 16 (2016), pp. 485–496.
- [18] V. H. SCHULZ, M. SIEBENBORN, AND K. WELKER, *Efficient PDE constrained shape optimization based on Steklov–Poincaré-type metrics*, SIAM Journal on Optimization, 26 (2016), pp. 2800–2819, <https://doi.org/10.1137/15m1029369>, <https://doi.org/10.1137/15m1029369>.
- [19] A. SHAMANSKIY AND B. SIMEON, *Mesh moving techniques in fluid-structure interaction: robustness, accumulated distortion and computational efficiency*, Computational Mechanics, 67 (2020), pp. 583–600, <https://doi.org/10.1007/s00466-020-01950-x>, <https://doi.org/10.1007/s00466-020-01950-x>.
- [20] S. SIVAPRASAD, A. SINGH, N. MANWANI, AND V. GANDHI, *The curious case of convex neural networks*, in Joint European Conference on Machine Learning and Knowledge Discovery in Databases, Springer, 2021, pp. 738–754.
- [21] F. TRÖLTZSCH, *Optimal Control of Partial Differential Equations*, American Mathematical Society, Apr. 2010, <https://doi.org/10.1090/gsm/112>, <https://doi.org/10.1090/gsm/112>.
- [22] S. TUREK AND J. HRON, *Proposal for numerical benchmarking of fluid-structure interaction between an elastic object and laminar incompressible flow*, in Fluid-structure interaction, Springer, 2006, pp. 371–385.
- [23] T. WICK, *Fluid-structure interactions using different mesh motion techniques*, Computers & Structures, 89 (2011), pp. 1456–1467.
- [24] J. XU AND K. YANG, *Well-posedness and robust preconditioners for discretized fluid–structure interaction systems*, Computer Methods in Applied Mechanics and Engineering, 100 (2015), pp. 69–91.
- [25] K. XU AND E. DARVE, *Adcme: Learning spatially-varying physical fields using deep neural networks*, 2020, <https://arxiv.org/abs/arXiv:2011.11955>.
- [26] A. YAZDANI, L. LU, M. RAISSI, AND G. E. KARNIADAKIS, *Systems biology informed deep learning for inferring parameters and hidden dynamics*, PLoS computational biology, 16 (2020), p. e1007575.